THE ROYAL SOCIETY FirstCite® e-publishing

Received 7 June 2000
Accepted 5 September 2001
Published online

Cryptic and conspicuous coloration in the pelagic environment

Sönke Johnsen†

Woods Hole Oceanographic Institution, Woods Hole, MA 02543-1049, USA

Despite the importance of cryptic and conspicuous coloration in pelagic ecosystems, few researchers have investigated the optimal reflectance spectra for either trait. In this study, the underwater radiance distribution in tropical oceanic water was modelled using measured inherent optical properties and radiative transfer calculations. The modelled light field was then used to predict the reflectance spectra that resulted in minimal or maximal object contrast as a function of depth, viewing angle, azimuth and solar elevation. The results matched commonly observed trends in the coloration of many pelagic organisms and showed that optimal coloration for either crypticity or conspicuity is a complex function of the parameters examined. The effects of viewing angle and depth were substantial and non-intuitive, showing that red coloration is most cryptic at depth. The effects of viewing azimuth were less significant and the effects of solar elevation were minor. White coloration and black coloration were equally cryptic/conspicuous when viewed from below. Although conspicuous objects viewed from below had the lowest contrast when viewed from a short distance, they had the longest sighting distances. The contrast of maximally conspicuous objects viewed from short distances was greatest at wavelengths displaced from the wavelength of maximum light penetration.

Keywords: camouflage; colour vision; ocean optics; visual predation

1. INTRODUCTION

Pelagic species are visually exposed to a degree not found in any other ecosystem, due to the simple fact that there are no physical objects to hide within or behind (McFall-Ngai 1990; Hamner 1996). This has led to the evolution of complex adaptations for camouflage including whole-body transparency (Chapman 1976; Johnsen & Widder 1998, 1999, 2001), mirrored sides (Denton 1970), countershading and counterillumination (Cott 1940; McAllister 1967; Denton *et al.* 1972; Kiltie 1988; Ferguson & Messenger 1991), morphological adaptations to minimize body profile (Seapy & Young 1986), and cryptic coloration (Endler 1978, 1990, 1991; Herring & Roe 1988; Muntz 1990; Fuiman & Magurran 1994). Conversely, several of these adaptations are also employed to increase visibility for sexual signalling, luring prey, and advertising chemical defences (Purcell 1980; Endler 1991; Bakker & Mundwiler 1992; Hanlon & Messenger 1996; Marshall 2000). Concurrent with these adaptations, complex visual abilities have evolved to break camouflage. These are generally contrast-increasing mechanisms and include ultraviolet (UV) vision, polarization vision, coloured ocular filters and offset visual pigments (Waterman 1981; Lythgoe 1984; Bowmaker & Kunz 1987; Muntz 1990; Loew *et al.* 1993; Browman *et al.* 1994; Shashar *et al.* 1998).

Unlike terrestrial systems, light in aquatic systems is strongly affected by the surrounding medium (Jerlov 1976; Kirk 1983; Mobley 1995). Therefore, the success or failure of either camouflage or a conspicuous signal depends not only on the visual capabilities of the viewer, but also on the depth of the viewed organism, the angle from which it is viewed, and the optical properties of the water (Munz & McFarland 1977; Endler 1991). Although cryptic coloration has been explored in considerable detail for aquatic systems with backgrounds containing significant physical structure (e.g. coral reefs, benthic and freshwater systems) (e.g. Endler 1978, 1983, 1991; Crook 1997), less work has been done on pelagic systems. Munz and McFarland and later Loew, Lythgoe, Partridge, and Marshall in various individual, and collaborative, studies have explored the visibility of underwater objects, all with the primary aim of understanding the relationship between visual spectral sensitivity and optical environment (e.g. Munz & McFarland 1973, 1977; Loew & Lythgoe 1978; Lythgoe 1984; Lythgoe & Partridge 1989; Loew & McFarland 1990; Marshall 2000). This study takes a different approach, in that it calculates the optimally cryptic and conspicuous coloration—as a function of viewing angle, depth, and solar elevation—from the underwater radiance distribution. In doing so, it lays a physical framework for future studies on underwater visibility that would also include the visual capabilities of the viewer.

2. MATERIAL AND METHODS

(a) *Factors affecting sighting distance underwater*

The visibility of an underwater object generally depends more upon its contrast than on its size (Mertens 1970; Hemmings 1975; Lythgoe 1979). The inherent contrast (contrast at zero distance) at wavelength λ is defined as

$$C_o(\lambda) = \frac{L_o(\lambda) - L_b(\lambda)}{L_b(\lambda)}, \tag{2.1}$$

where $L_o(\lambda)$ is the radiance of the object and $L_b(\lambda)$ is the radiance of the background, both viewed a short distance from the object (Hester 1968; Mertens 1970; Jerlov 1976). The absolute value of contrast decreases exponentially with distance according to

† Present address: Department of Biology, Box 90338, Duke University, Durham, NC 27708, USA (sjohnsen@duke.edu)

$$|C(\lambda)| = |C_o(\lambda)| \times e^{(K_L(\lambda) - c(\lambda))d}, \quad (2.2)$$

where $|C(\lambda)|$ is the absolute value of apparent contrast at distance d from the object, $K_L(\lambda)$ is the attenuation coefficient of the background radiance, and $c(\lambda)$ is the beam attenuation coefficient of the water (Mertens 1970; Jerlov 1976). Let $C_{min}(\lambda)$ be the minimum contrast for object detection for a given visual system. Substituting $C_{min}(\lambda)$ for $C(\lambda)$ and solving equation (2.2) for d gives

$$d(\lambda) = \frac{\ln\left(\left|\frac{C_o(\lambda)}{C_{min}(\lambda)}\right|\right)}{c(\lambda) - K_L(\lambda)}. \quad (2.3)$$

(Note that the sign change in the denominator and the inverse in the log function cancel.)

This distance $d(\lambda)$ is the maximum distance at which the object is detectable, and is referred to hereafter as the sighting distance, or $d_{sighting}(\lambda)$. This distance depends on the product of two factors:

(i) $\ln\left(\left|\frac{C_o(\lambda)}{C_{min}(\lambda)}\right|\right)$,

the relationship of the inherent contrast of the object to the minimum contrast threshold of the viewer (referred to hereafter as the 'contrast factor'), and

(ii) $\frac{1}{c(\lambda) - K_L(\lambda)}$,

the specific optical properties of the water that determine how rapidly the inherent contrast is attenuated (referred to hereafter as the 'penetration factor'). Although object size also affects sighting distance, particularly for smaller objects and/or greater distances (Aksnes & Giske 1993; Giske *et al.* 1994), it is not considered in this study.

(b) *Calculation of reflectance spectra for minimal and maximal inherent contrast*

In the simplifying (but biologically common and useful) case of objects that reflect diffusely (i.e. in a non-mirror-like fashion)

$$L_o(\lambda) = \frac{R(\lambda)E(\lambda)}{\pi}, \quad (2.4)$$

where $R(\lambda)$ is the bihemispherical reflectance of the object (diffuse reflectance of diffuse illumination) and $E(\lambda)$ is the irradiance at the object's surface (Mertens 1970; Palmer 1995). Substituting equation (2.4) into equation (2.1) gives

$$C_o(\lambda) = \frac{R(\lambda)E(\lambda)}{\pi L_b(\lambda)} - 1. \quad (2.5)$$

Setting the inherent contrast to zero and solving for equation (2.5) for $R(\lambda)$ gives

$$R_{cryptic}(\lambda) = \frac{\pi L_b(\lambda)}{E(\lambda)}. \quad (2.6)$$

This $R(\lambda)$ is the reflectance that results in zero contrast at wavelength λ and is referred to hereafter as $R_{cryptic}(\lambda)$.

For conspicuous coloration, the absolute value of inherent contrast is maximal. Because $0 \leqslant R(\lambda) \leqslant 1$, from equation (2.5) $|C_o(\lambda)|$ is maximal when $R(\lambda) = 0$ or $R(\lambda) = 1$. When $R(\lambda) = 0$,

$$|C_o(\lambda)| = \left|\frac{0 \times E(\lambda)}{\pi L_b(\lambda)} - 1\right| = 1. \quad (2.7)$$

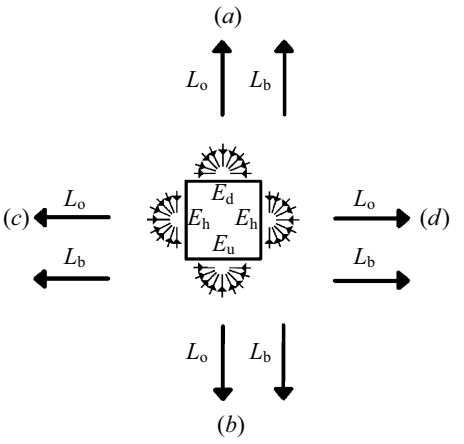

Figure 1. The four different viewing angles that were analysed. (*a*) Viewing a horizontal surface from above, where the object radiance is proportional to the downwelling irradiance (denoted by a cluster of inward pointing arrows), and the background radiance is the upward radiance. (*b*) Viewing a horizontal surface from below, where the object radiance is proportional to the upwelling irradiance, and the background radiance is the downward radiance. (*c*) Horizontal viewing of a vertical surface in the azimuth of the sun, where the object radiance is proportional to the horizontal irradiance opposite the solar azimuth, and the background radiance is the horizontal radiance in solar azimuth. (*d*) Horizontal viewing of a vertical surface in the azimuth opposite the sun, where the object radiance is proportional to the horizontal irradiance in solar azimuth, and the background radiance is the horizontal radiance opposite solar azimuth. The dark circle denotes the sun (which is in the plane of the figure). The horizontal line denotes the sea surface.

When $R(\lambda) = 1$,

$$|C_o(\lambda)| = \left|\frac{E(\lambda)}{\pi L_b(\lambda)} - 1\right|. \quad (2.8)$$

Therefore, when $E(\lambda)/(\pi L_b(\lambda)) > 2$, maximal contrast is achieved when $R(\lambda) = 1$. When $E(\lambda)/(\pi L_b(\lambda)) < 2$, maximal contrast is achieved when $R(\lambda) = 0$. From equation (2.6), $R_{cryptic}(\lambda) = \frac{\pi L_b(\lambda)}{E(\lambda)}$,

$$R_{conspicuous}(\lambda) = 1, \text{ when } R_{cryptic}(\lambda) < \frac{1}{2}, \text{ and} \quad (2.9)$$

$$R_{conspicuous}(\lambda) = 0, \text{ when } R_{cryptic}(\lambda) > \frac{1}{2}. \quad (2.10)$$

Therefore, the optimal reflectance spectra for crypticity and conspicuity depend on the irradiance at the object's surface and the radiance in the viewer's line of sight. For this study, four different viewing angles were examined: (i) viewing from directly above, (ii) viewing from directly below, (iii) viewing horizontally in the solar azimuth, and (iv) viewing horizontally opposite the solar azimuth (figure 1). For each viewing angle, the viewed surface was assumed to be perpendicular to the viewing angle.

(c) *Calculation of underwater radiances and irradiances*

Although spectral measurements of radiance at selected angles have been made (Munz & McFarland 1977; Endler 1991; Marshall 2000), very few high-resolution measurements over the entire sphere exist (reviewed by Jerlov 1976; Mobley 1995). Because high-resolution angular data were required to calculate irradiances, and because the goal of the study was to predict general trends, not to exactly match a given location, an alternative approach was taken. With the exception of downwelling irradiance and upward radiance, underwater spectral and spatial radiance distributions were not measured, but instead were modelled using measured inherent optical properties and a sophisticated radiative transfer software package (Hydrolight 4.1, Sequoia Scientific). Given the depth profiles of the absorption coefficient, beam attenuation coefficient, and chlorophyll concentration, the software calculates the underwater radiance distribution as a function of depth and wavelength (from 350 to 800 nm), taking into account solar elevation and azimuth, atmospheric parameters, sea-surface conditions, chlorophyll fluorescence, and Raman scattering by the water. Raman scattering is inelastic scattering of photons by water molecules, and therefore converts a small fraction of incident photons to photons of lower energy and therefore longer wavelength (Stavn & Wiedemann 1988; Marshall & Smith 1990; Mobley 1995; Gordon 1999). Raman scattering is also spatially isotropic (as opposed to scattering by particles which is strongly peaked in the forward direction). Though unimportant near the surface, inelastically scattered light becomes increasingly important at greater depths due to the heavy attenuation of long-wavelength 'solar' photons. The ability of the software to accurately model radiance distributions has been validated by *in situ* measurements of selected radiances and irradiances in numerous studies (e.g. Mobley *et al.* 1993; Maffione *et al.* 1998; Stramska *et al.* 2000). The agreement between modelled and measured radiances is particularly good in tropical oceanic waters, because the vast majority of the light attenuation is due to the water itself, which is easily characterized and well understood.

Depth profiles of inherent optical properties (IOPs) and chlorophyll concentration from tropical oceanic water (approximately Jerlov oceanic type I) were obtained from Dr Andrew Barnard, Dr Scott Pegau and Dr Ronald Zaneveld (College of Oceanic and Atmospheric Sciences, Oregon State University, Corvallis, OR, USA), who collected them using a dual path, multiband absorption/ attenuation meter (ac-9, Wetlabs Inc.) and fluorometer in the Equatorial Pacific (10.05 local time, 30 April 1996; 0°0′ N, 177°21′ W). Absorption and beam attenuation coefficients (at 412, 440, 488, 510, 532, 555, 650 and 676 nm) and chlorophyll concentration were measured at 1 m intervals to a depth of 138 m. Absorption and attenuation measurements were not taken at any UV wavelengths, and cannot be taken with this instrument, precluding the possibility of modelling the UV radiance distribution. This is unfortunate, considering the prevalence of UV vision in near-surface species (reviewed by Johnsen & Widder 2001).

Underwater radiance distributions were calculated from zero to 100 m depth at 10 m intervals for two solar elevations, chosen to approximate to two extremes of skylight radiance distribution. A solar elevation of 80° (above the horizon), generally found near noon, results in an approximately (but not perfectly) symmetrical radiance distribution. A solar elevation of 10°, generally found near sunset, results in a maximally asymmetrical radiance distribution. These two elevations were chosen to study the effects of solar elevation on azimuthal predictions, not to examine the effect of the different sky irradiance spectra at twilight (Munz & McFarland 1977). For each distribution, the sky was assumed to be cloudless and the sea state was assumed to be calm. The sky irradiance was calculated using the RADTRAN model (Gregg & Carder 1990), and the sky radiance distribution was calculated using the model given in Harrison & Coombes (1988). Both models account for atmospheric effects, such as the reddening of the sun as it approaches the horizon, and are well established. Figure 2 shows the sky irradiance at the two solar elevations. Pure water absorption was taken from Pope & Fry (1997), and the scattering phase function was Petzold's average particle (Petzold 1977). Chlorophyll fluorescence was calculated from chlorophyll absorption taken from Prieur & Sathyendranath (1981) and a fluorescence efficiency of 0.02.

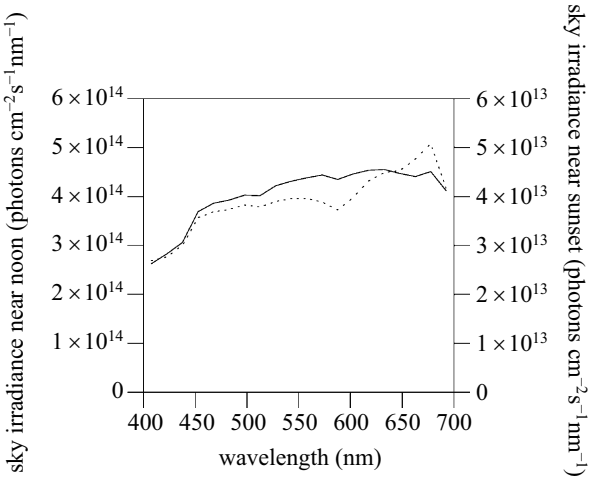

Figure 2. Modelled sky irradiance near noon (solid line, left *y*-axis) and near sunset (dotted line, right *y*-axis). The humidity is 80% and visibility is 15 km. The irradiance near sunset is approximately one-tenth of the irradiance near noon and is slightly richer in long wavelengths.

At each depth, radiance was calculated from 400 to 700 nm at 15 nm intervals with an angular resolution of 15° (azimuth) by 10° (elevation). From the radiance distributions, vector irradiances were calculated for the following vectors: upward, downward, horizontal in the solar azimuth, horizontal opposite the solar azimuth.

(d) *Calculation of contrast factor for white and black ventral surfaces viewed from below and horizontally*

Preliminary analyses showed that the predicted cryptic reflectance for an object viewed from below, $R_{\mathrm{cryptic}}(\lambda)$, was generally several orders of magnitude greater than the maximum realizable value of unity. Substituting equation (2.6) into equation (2.5) and setting the reflectance to unity gives

$$C_{\mathrm{o}}(\lambda) = \frac{1}{R_{\mathrm{cryptic}}(\lambda)} - 1, \qquad (2.11)$$

which, for large values of $R_{\mathrm{cryptic}}(\lambda)$ approximates to −1. When reflectance equals zero, the inherent contrast equals −1. Therefore, a white ventral surface may not have a significantly lower sighting distance than a black ventral surface. This was examined by calculating the contrast factor

$$\ln\left(\left|\frac{C_{\mathrm{o}}(\lambda)}{C_{\mathrm{min}}(\lambda)}\right|\right)$$

for reflectances of unity and zero. The minimum contrast threshold was set to 0.02, the value for human vision in well-lit surface waters (Lythgoe 1979). For comparison, the minimum contrast thresholds in well-lit environments are also known for the following aquatic species: goldfish (*Carassius auratus*, 0.009–0.05), cod (*Gadus morhua*, 0.02), rudd (*Scardinius erythrophthalamus*, 0.03–0.07), roach (*Rutilus rutilus*, 0.02), bluegill (*Lepomis macrochirus*, 0.003–0.007), and Japanese common squid (*Todarodes pacificus*, 0.006) (Lythgoe 1979; Douglas & Hawryshyn 1990; Siriraksophon *et al.* 1995). Because a ventral surface can be viewed from angles other than from directly below, the contrast factor was also calculated in the limiting case of viewing a ventral surface horizontally (edge-on). Contrast factors for intermediate viewing angles are bounded by these two cases.

(e) *Calculation of penetration factor as a function of depth and viewing angle*

The penetration factor is a function of the beam attenuation coefficient, $c(\lambda)$, which is independent of the viewing angle, and the attenuation coefficient of background radiance, $K_L(\lambda)$, which depends upon the viewing angle (see above). For the downward viewing angle, $K_L(\lambda) = -K_{L_u}(\lambda)$, where $K_{L_u}(\lambda)$ is the attenuation coefficient of upward radiance. For the upward viewing angle, $K_L(\lambda) = K_{L_d}(\lambda)$, the attenuation coefficient of downward radiance. For horizontal viewing, $K_L(\lambda) = 0$. Therefore, $1/(c(\lambda) + K_{L_u}(\lambda))$, $1/(c(\lambda) - K_{L_d}(\lambda))$, and $1/(c(\lambda))$, were evaluated as a function of depth. The beam attenuation coefficients were obtained from the measured profiles; $K_{L_u}(\lambda)$ and $K_{L_d}(\lambda)$ were calculated from the modelled radiance distributions.

(f) *Calculation of optimal reflectance for crypticity using measurements of radiance and irradiance*

Although the high angular resolution measurements needed for calculation of horizontal and upwelling irradiance do not exist, downwelling irradiance and upward radiance data were taken concurrently with the IOP profiles described above. Ten profiles were obtained using a multispectral radiometer (SPMR, Satlantic Inc., Halifax, Canada) that simultaneously measured downwelling irradiance (at 413, 444, 490, 532, 556, 590 and 670 nm) and upward radiance (at 413, 444, 490, 533, 590, 619 and 684 nm). The bandwidth of the filters was 10 nm (full width at half maximum). The shared measurements (at 413, 444, 490, 532 and 590 nm) were inserted into equation (2.6) to compare with the modelled prediction for cryptic reflectance when viewed from above. To obtain a long-wavelength prediction, the ratio

$$\pi \frac{L(684)}{E(670)}$$

was plotted at an intermediate wavelength of 677 nm. This is somewhat inaccurate, although the irradiance and radiance curves are relatively flat in this spectral region (see § 3).

3. RESULTS

(a) *Modelled irradiance and radiance in the four viewing angles*

The modelled irradiances and radiances in the four viewing angles displayed the typical predominance of blue wavelengths found in oceanic water, with approximately constant irradiance from 400 to 500 nm, a decrease for wavelengths greater than 575 nm, and an increasingly prominent peak at 675 nm due to chlorophyll fluorescence (figure 3). The decrease in intensity at longer wavelengths was less dramatic for upward radiances and upwelling irradiances. The attenuation of long wavelengths (> 575 nm) with depth was initially high, but then dropped to values comparable to the attenuation of shorter wavelengths, due to the increasing proportion of inelastically scattered light. The ratio of the upward to downward intensity (irradiance and radiance) at longer wavelengths approached unity at longer wavelengths and increasing depth due to the isotropic nature of inelastic scattering. Downward radiance was far higher than upwelling irradiance at both solar elevations, though the difference was far less at the lower elevation (figure 3*c*,*d*). In all other viewing angles, the irradiance was higher than the radiance in the opposite vector (figure 3*a*,*e*,*f*). The modelled spectra near sunset (solar elevation of 10°) had irradiance values approximately one-tenth of those near noon at all viewing angles. Aside from this, they closely approximated the near-noon spectra and are not shown.

The measured upward radiance and downwelling irradiance matched the modelled values quite closely for wavelengths equal to or less than 590 nm, and followed a similar pattern at longer wavelengths (figure 3*b*). However, more long-wavelength light at depth was measured than predicted by the model.

(b) *Predicted reflectance spectra for crypticity*

For an object viewed from above near noon, the predicted reflectance spectra from 400 to 550 nm were essentially constant as a function of depth and inversely proportional to wavelength (figures 4*a* and 5*a*). For wavelengths of more than 550 nm, the predicted reflectance increased, from a relatively low value at the surface, to nearly unity at a depth of 100 m. The predicted reflectances near sunset approximated to those near noon and are only shown as colour swatches (figure 5*b*). The predicted reflectances from the SPMR measurements closely approximated to the modelled reflectances for wavelengths equal to or less than 590 nm (figure 4*b*). At 677 nm, the predictions from the measurements were lower than the predictions from the model, although they followed the same basic pattern.

For an object viewed from below near noon, the predicted reflectances at the surface were orders of magnitude greater than unity and proportional to wavelength (figures 4*c* and 5*a*). With increasing depth, the predicted reflectances decreased slightly from 400 to 575 nm and dramatically from 575 to 700 nm. Near sunset, the predicted reflectances at the surface were lower by one to two orders of magnitude, but, with increasing depth, the reflectances increased at short wavelengths and decreased at long wavelengths to approximate the predicted noon reflectances at 100 m (figures 4*d* and 5*b*).

The predicted reflectance for horizontal viewing near noon depended on the viewing azimuth relative to the solar azimuth. For objects viewed in the solar azimuth (i.e. with the sun behind the object) at the surface, the predicted reflectances were relatively high and inversely proportional to wavelength (figures 4*e* and 5*a*). With increasing depth, short-wavelength reflectance decreased and long-wavelength reflectance increased to a maximum of unity. For objects viewed opposite the solar azimuth

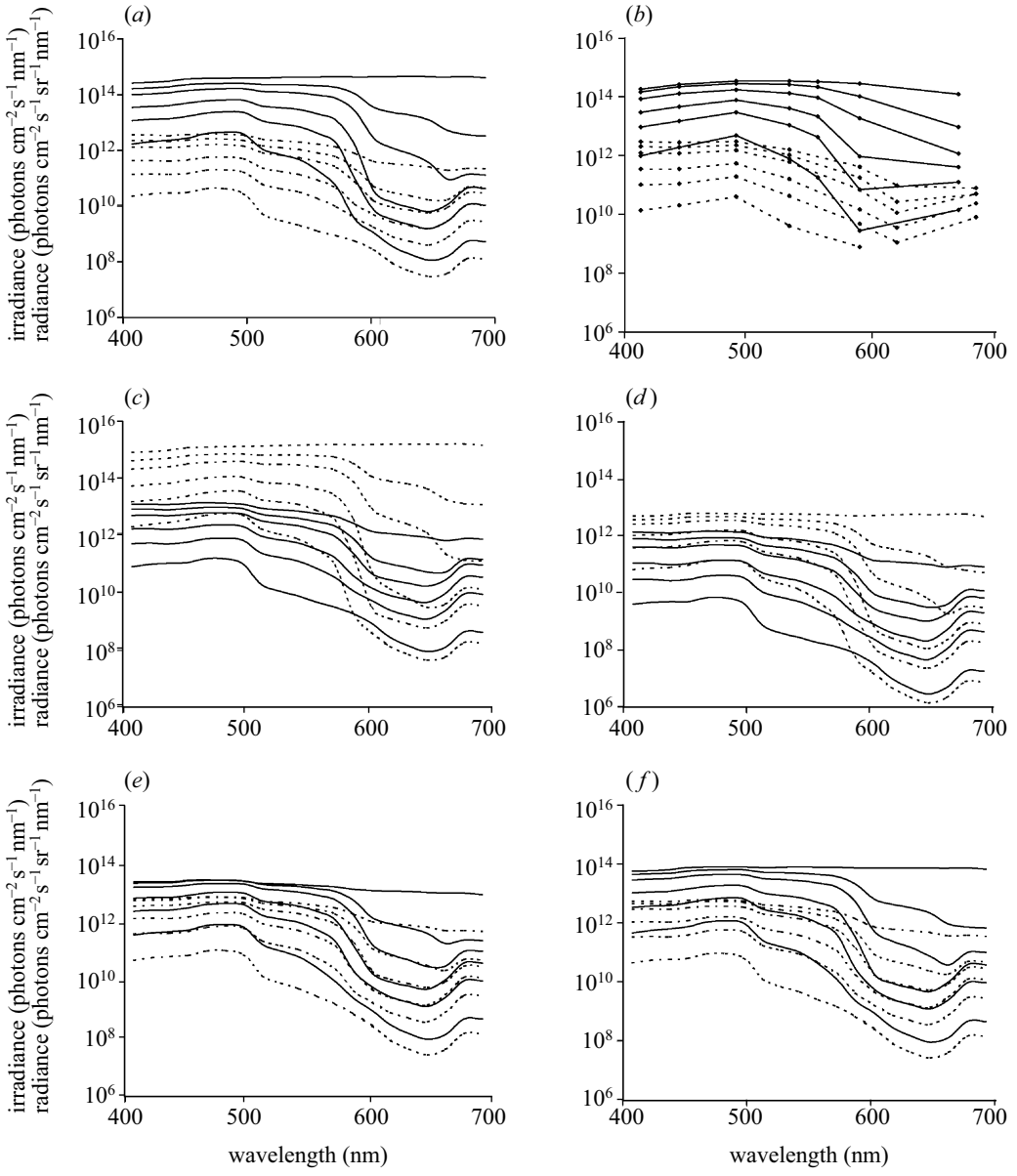

Figure 3. Irradiance (solid lines) and radiance (dashed lines) in the four viewing angles modelled from measured inherent optical properties and chlorophyll concentrations from the Equatorial Pacific. Depths are 0, 10, 20, 40, 60 and 100 m. Upward radiance, downwelling irradiance (*a*) viewed from above and (*b*), from measurements. Downward radiance, upwelling irradiance (*c*) viewed from below and (*d*) with a solar elevation of 10°. (*e*) Horizontal radiance in solar azimuth, horizontal irradiance opposite solar azimuth (viewing in solar azimuth). (*f*) Horizontal radiance opposite solar azimuth, horizontal irradiance in solar azimuth (viewing opposite solar azimuth). (*b*) Measured values of downwelling irradiance and upward radiance from the same site at 10.05. The first depth is 3 m, rather than 0 m. Radiance values at 619 and 684 nm at 100 m depth were below the noise level of the radiometer and are not shown. The lines connecting the data points in (*b*) do not necessarily imply a linear interpolation. Therefore, for example, the radiance at 620 nm cannot be compared with interpolated irradiance at 620 nm.

(i.e. with the sun behind the viewer), the pattern was similar to that for objects viewed from above, with the lower bound *ca*. 10-fold greater and the upper bound still equal to unity (figures 4*f* and 5*a*). The predicted reflectances near sunset approximated those at noon (figure 5*b*).

(c) *Predicted reflectance spectra and sighting distances for conspicuity*

The predicted reflectance spectra for conspicuous coloration are not explicitly shown, but are implied by the crypticity predictions (figure 4). Where the predicted reflectance for crypticity was below the $R = \frac{1}{2}$ line (shown on the graphs), the predicted reflectance for conspicuity is unity. Where the predicted reflectance was above the $R = \frac{1}{2}$ line, the predicted reflectance is zero. When viewed from above, the predicted reflectance spectra were constant at unity in shallow water, with a cut-off to a reflectance of zero at increasingly shorter wavelengths with increasing depth (figures 4*a* and 5*c*,*d*). When viewed from below, the predicted reflectance spectra were zero at all depths (figures 4*c*,*d* and 5*c*,*d*). When viewed horizontally in the solar azimuth, the predicted spectra were high at long wavelengths in shallow water, shifting to high at short wavelengths with increasing depth (figures 4*e* and 5*c*,*d*).

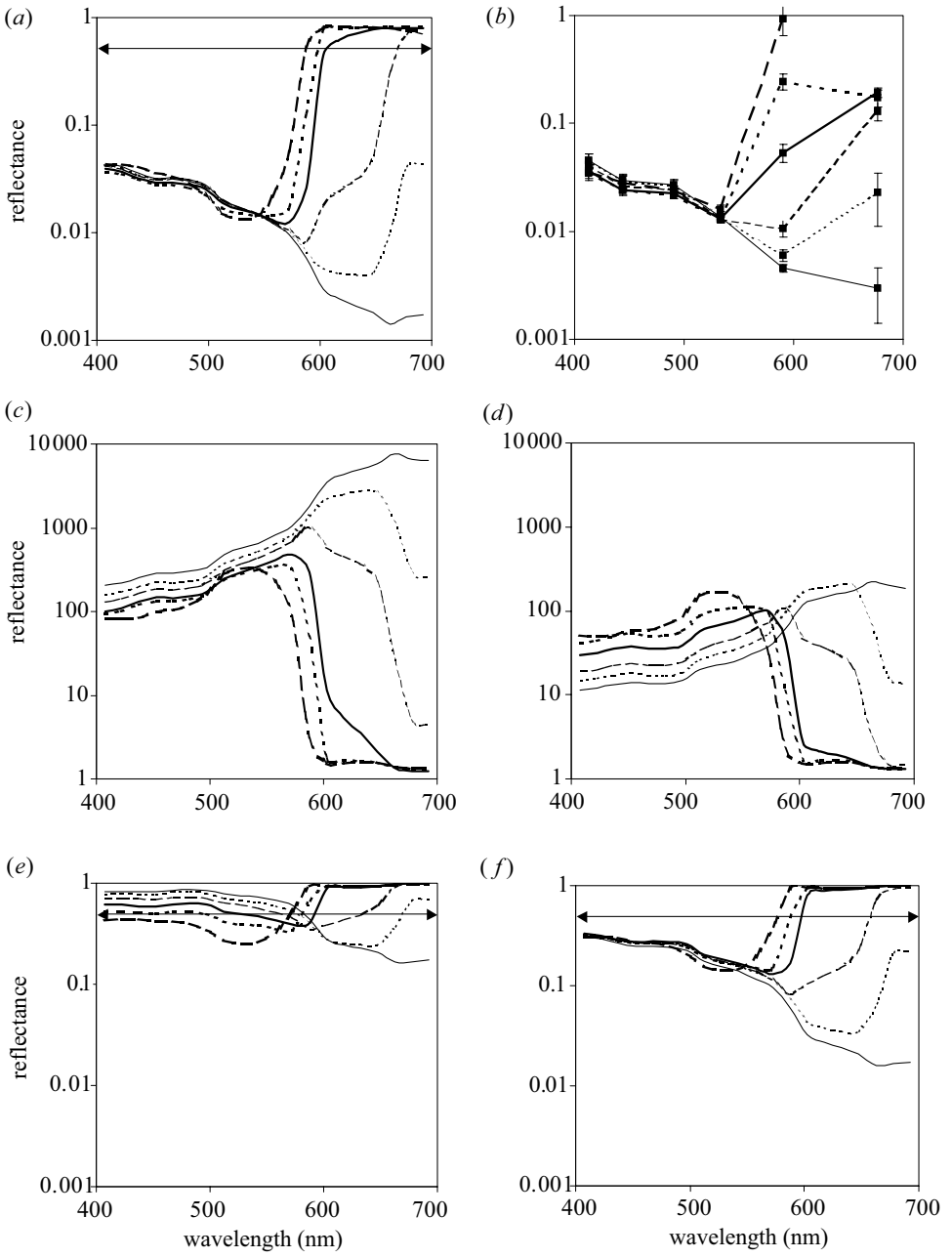

Figure 4. Predicted reflectance spectra of an object with zero inherent contrast for six depths and four viewing angles. (*a*) Object viewed from above and (*b*) from measurements. (*c*) Object viewed from below and (*d*) object viewed from below near sunset. (*e*) Object viewed horizontally in solar azimuth and (*f*) opposite solar azimuth. Predictions are based on radiance distributions modelled from measured inherent optical properties and chlorophyll concentrations from a site in the Equatorial Pacific. Solar elevation is 80° (unless otherwise stated). The double-arrowed line in each plot denotes $R = \frac{1}{2}$. Solid lines represent 0 m, dotted lines, 10 m, dashed lines, 20 m, thick solid lines, 40 m, thick dotted lines, 60 m and thick-dashed lines, 100 m. Note that the *y*-axis scale for objects viewed from below is different from the scale for the other three viewing angles. (*b*) Predicted reflectances using 10 measurements of downwelling irradiance and upward radiance. The first depth is 3 m, rather than 0 m. The value at 677 nm at 100 m depth was below the noise level of the radiometer and is not shown. Error bars denote standard deviation.

When viewed horizontally opposite the solar azimuth, the predicted reflectance spectra were essentially identical to those obtained for the downward viewing angle (figures 4*f* and 5*c*,*d*). For all viewing angles, the predictions near noon and near sunset were not significantly different (figure 5*c*,*d*).

Objects with conspicuous coloration had the highest inherent contrast when viewed from above, but the longest sighting distances when viewed from below at all depths (figure 6*a*,*b*). When viewed horizontally, objects had intermediate inherent contrasts and sighting distances, with both values slightly higher for objects viewed opposite the solar azimuth (figure 6*c*,*d*). When viewed from below in shallow water, the sighting distance for conspicuously coloured objects was linearly proportional to wavelength. At depths greater than 40 m, objects were most distantly visible at *ca.* 590 nm. When viewed at any other angle, conspicuous objects were most distantly visible at *ca.*

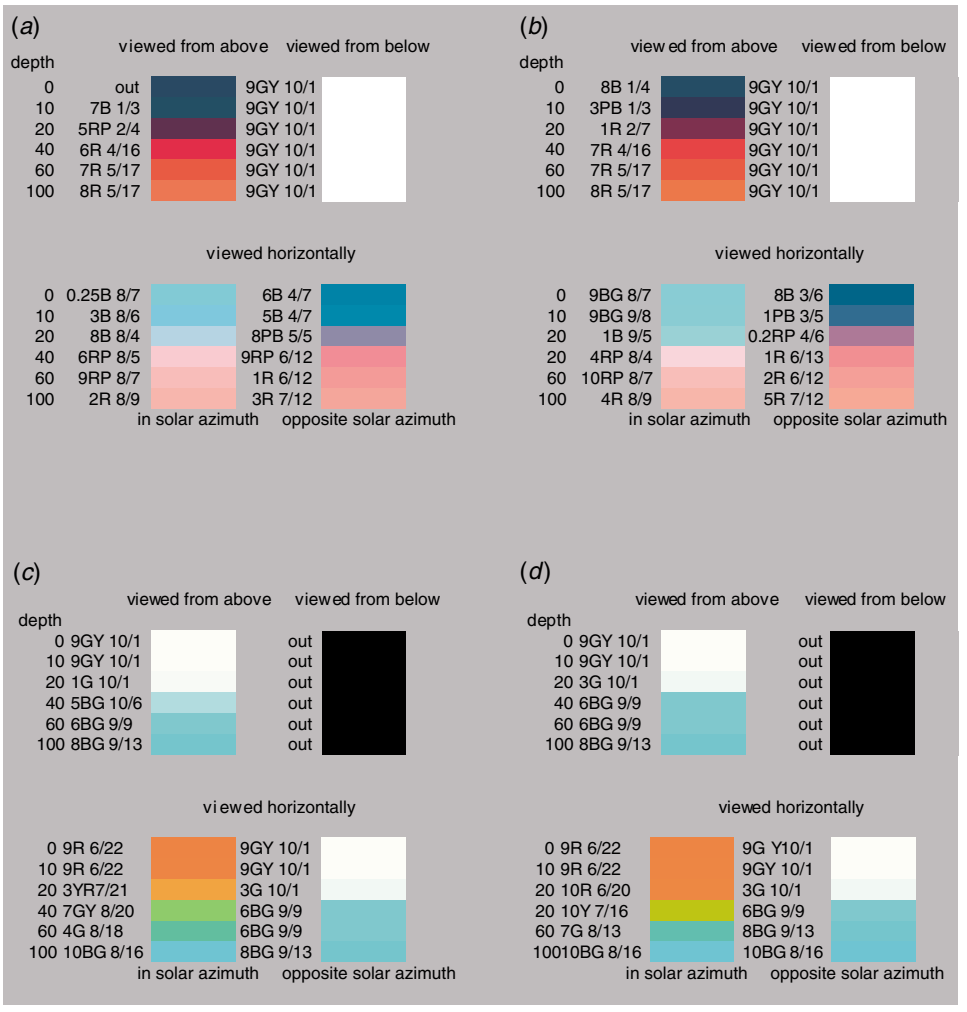

Figure 5. (*a*,*b*) The predicted reflectance spectra for crypticity and (*c*,*d*) conspicuousness, represented as colour swatches. Solar elevations in (*a*) and (*c*) are 80° and in (*b*) and (*d*) are 10°. Reflectance spectra were converted to CIE XYZ coordinates using standard methods (Wyszecki & Stiles 1982), converted to RGB coordinates using colour conversion software (Munsell Conversion Program, GretagMacbeth Inc.), and then printed on a CMYK printer using colour management software (ICM 2.0, Microsoft Inc.). Colour swatches match the appearance of an organism with the predicted reflectance spectrum when both are viewed by a human observer under normal daylight (CIE D_{65} standard illuminant). Due to the limited colour range of printers, the match is not perfect. Therefore, the Munsell notation is given for each colour swatch, for those with access to the 'Munsell book of colour', which has a larger colour range.

500 nm. At these viewing angles, the wavelength of highest apparent contrast decreased with increasing distance from the object. The predictions near sunset were not significantly different from those at noon and are not shown.

(d) *Contrast factors for white and black ventral surfaces viewed from below and horizontally*

When viewed from directly below, the contrast factors for white and black ventral surfaces were not significantly different at any wavelength at shallow depths and only different at longer wavelengths at deeper depths (figure 7*a*). When viewed horizontally, the contrast factor for a white ventral surface was *ca.* 80% of the contrast factor for a black ventral surface from 400 to 575 nm for all depths (figure 7*b*). For wavelengths greater than 575 nm, the ratio dropped as depth increased.

(e) *Penetration factor as a function of depth and viewing angle*

The penetration factor increased slightly with depth at shallow depths and more rapidly with depth at greater depths (figure 8). For the downward and horizontal viewing angles, the penetration factor was greatest at the wavelength of greatest light penetration (figure 8*a*,*c*). For the upward viewing angle, the penetration factor was generally higher than at the other two viewing angles and was approximately independent of wavelength at shallow depths (figure 8*b*). At greater depths, the penetration factor was high for $\lambda < 575$ nm, and low for $\lambda > 575$ nm, peaking at $\lambda = 575$ nm. The predictions near sunset were not significantly different from those at noon and are not shown.

4. DISCUSSION

(a) *General*

The results of this study show that the visibility of a coloured marine organism depends critically and non-intuitively on a number of parameters. Many of the non-intuitive results are primarily due to five factors. First, the predicted colours depend on the irradiance in one direction

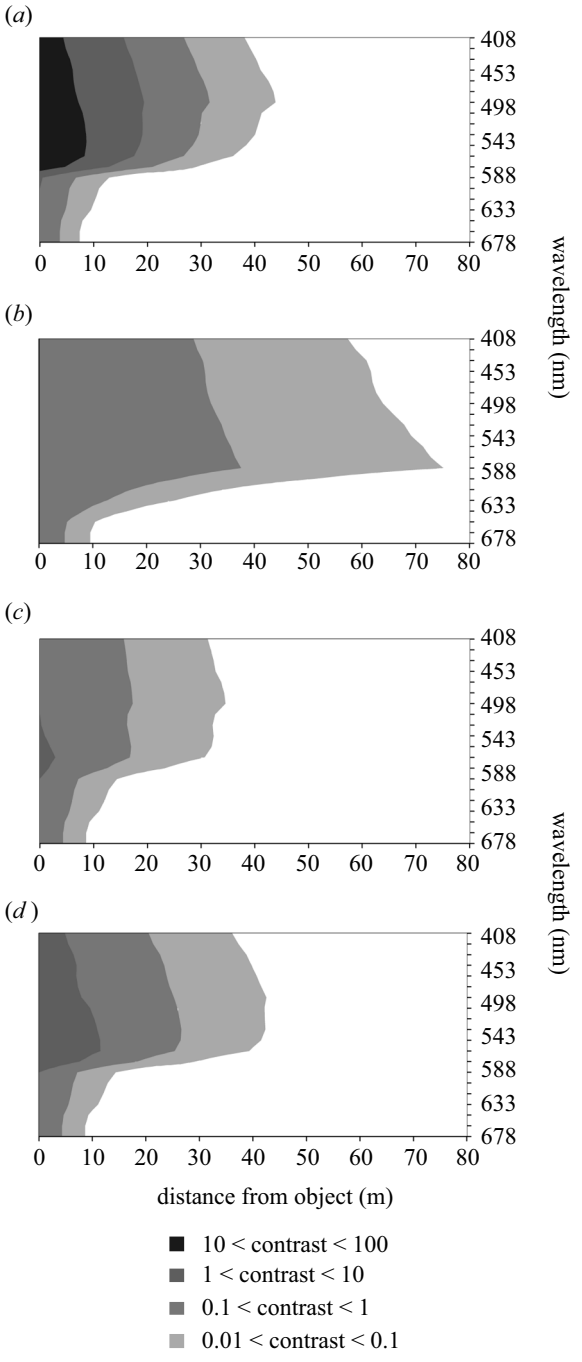

Figure 6. Decrease of the absolute value of the apparent contrast of a conspicuously coloured organism as a function of distance and wavelength near noon. The organism is at a depth of 40 m. Object viewed (*a*) from above, (*b*) from below, (*c*) horizontally (in solar azimuth) and (*d*) horizontally (opposite solar azimuth).

and the radiance in the opposite direction. Because irradiance includes light from an entire hemisphere, its spectrum is different from radiance in the same direction. Therefore, for example, a cryptic lateral surface should be blue rather than white, because the incident irradiance contains light from above and therefore is richer in longer and shorter wavelengths ('purpler') than the horizontal radiance. Second, the light field is highly diffuse and dominated by absorption, which minimizes the effects of solar elevation and viewing azimuth. Third, inelastic scattering creates a long-wavelength radiance distribution at a depth that is both spatially isotropic and far brighter than would be predicted by extrapolating surface attenuation coefficients. Fourth, the attenuation of contrast depends strongly on viewing angle, and is not always least at the wavelength of greatest light penetration. Finally, the contrast factor is proportional to the *logarithm* of the inherent contrast, but the penetration factor is proportional to the *reciprocal* of the difference of the attenuation coefficients. Therefore, changes in the attenuation coefficients are likely to have a larger effect on the sighting distance than equal changes in the inherent contrast, particularly if the changes result in approximately similar attenuation coefficients.

Although some artificial optical systems can directly measure the radiance at small wavelength intervals (e.g. spectroradiometers), no biological visual system is known to function in this fashion. Instead, visual systems integrate radiance over the spectral ranges of 1–10 visual pigments (Bowmaker 1990; Marshall *et al.* 1999; Muntz 1999). For this reason, two lights with different spectra (known as metamers) can induce the same colour stimulus for a given viewer (Wyszecki & Stiles 1982). Given this, one might assume that the contrast of a cryptic organism need only satisfy

$$\int C(\lambda)\, V_i(\lambda)\, \mathrm{d}\lambda = 0 \qquad (3.1)$$

for each photoreceptor (where $V_i(\lambda)$ is the visual response curve of the photoreceptor), rather than the more stringent requirement of zero contrast for each wavelength in the visible region. However, a contrast spectrum that satisfies equation (3.1) for one visual system is unlikely to satisfy it for a different system with different visual pigments, unless the contrast actually is zero for all relevant wavelengths (see Appendix A). Given that marine visual systems (particularly those of teleosts, crustaceans and cephalopods) present a diverse array of spectral responses (Bowmaker 1990; Marshall *et al.* 1999; Muntz 1999), any organism interacting with multiple species is unlikely to be maximally cryptic or conspicuous unless the contrast is zero for all the wavelengths where sufficient illumination for vision exists, even if all the visual systems are monochromatic. In essence, multiple monochromatic visual systems with different responses comprise a form of colour vision. This fact extends the predictions of this study to rod-based monochromatic systems, and therefore includes a larger number of species and visual systems that can function in lower illumination.

An important factor to consider in the following discussion of the effects of the various parameters on the predictions is that the wavelength and intensity sensitivity of the minimum contrast threshold is poorly understood for most marine species (Douglas & Hawryshyn 1990). This limitation does not affect the predicted reflectance spectra or contrast attenuation functions, but probably does affect the importance of contrast at different wavelengths and illumination levels for a given visual system. Another factor to consider is that, for species with very low minimum contrast thresholds, the sighting distances (figure 6) are long enough that the size of the object also becomes important (Aknes & Giske 1993).

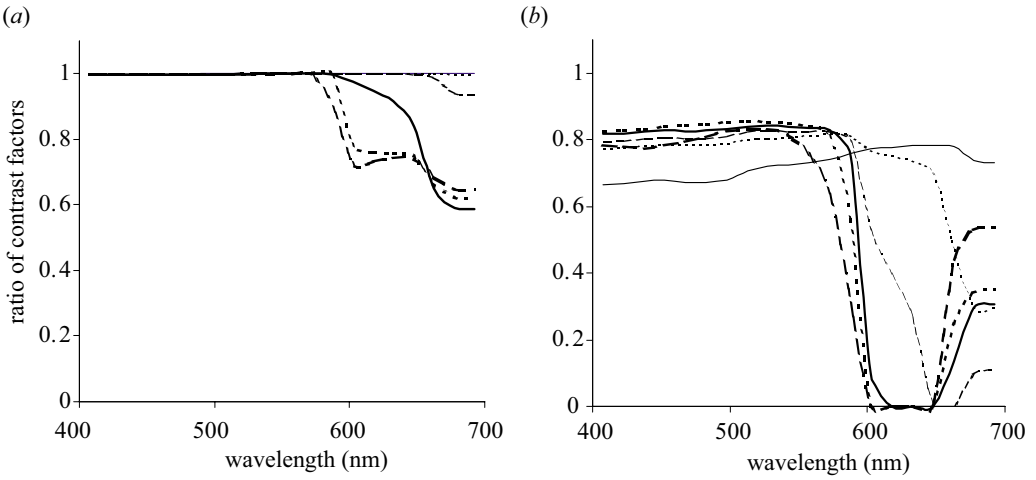

Figure 7. The ratio of the contrast factors for a white (most cryptic) and a black (least cryptic) ventral surface viewed from (*a*) directly below and (*b*) horizontally. A ratio of unity indicates that the white and black ventral surfaces are equally cryptic.

(**b**) *Effects of depth*

The relationship between depth and predicted coloration was relatively independent of depth at short wavelengths and extremely dependent on depth at long wavelengths. Because the predictions for the upward viewing angle are essentially constant (since the predicted cryptic reflectances are always greater than unity), reflectance spectra predictions are essentially independent of depth for wavelengths less than *ca.* 550 nm, except for horizontal viewing in the solar azimuth, where the depth effect was relatively minor. Therefore, if an individual is viewed by species whose spectral sensitivity is limited to wavelengths less than 550 nm, a single reflectance spectrum is successfully cryptic or conspicuous over a large range of depths, though only for one viewing angle.

The extreme depth dependence at long wavelengths is due to two factors: (i) inelastic scattering, and (ii) chlorophyll fluorescence. In inelastic scattering, a photon is scattered and its wavelength is increased (Stavn & Wiedemann 1988; Marshall & Smith 1990). In chlorophyll fluorescence, a small portion of light absorbed by phytoplankton is re-emitted at *ca.* 675 nm. As depth increases, and long wavelength photons are heavily attenuated relative to short wavelength photons (due to absorption by water and chlorophyll), inelastically scattered light and fluorescence contribute an increasing proportion of underwater radiance at long wavelengths (Stavn & Wiedemann 1988; Marshall & Smith 1990). Raman scattering plays a particularly important role in the spatial structure of long-wavelength light at depth. Marshall & Smith (1990) and others have measured the diffuse reflectance (E_u/E_d) on long-wavelength light as a function of depth and have shown that its dramatic increase (from 4 to 50% at 590 nm at 140 m) can be closely modelled by the influence of Raman scattering. Even at the surface, where solar light levels are maximal, Raman scattering increases the upward radiance by 10–15%, even at low wavelengths (Gordon 1999). However, it must be emphasized that the ocean at depth is overwhelmingly blue, with or without Raman scattering. It is the high irradiance reflectance (which implies an isotropic light field), not high levels of red light, which leads to the high predicted cryptic reflectances. Though Raman scattering increases the long-wavelength light at depth by many orders of magnitude, it is still quite dim and may be undetectable.

The predicted cryptic colours approximate some generally observed trends in the coloration of oceanic species. Numerous reviews of oceanic zooplankton and nekton have noted the blue coloration of near-surface species and the red coloration of deeper dwelling species (Cott 1940; Herring 1967, 1973; Herring & Roe 1988), though of course there are many exceptions. While the blue coloration observed near the surface is probably closely related to the concepts and predictions outlined in this study, the red coloration at depth is more problematic. The whole-body red coloration seen at depths greater than 400 m, where environmental red light is almost certainly below the threshold of vision, is generally considered to be a defence against directed bioluminescence (Herring & Roe 1988; McFall-Ngai 1990). Because the spectrum of bioluminescence is generally void of red wavelengths (Widder *et al.* 1983), red surfaces are not visible to species using bioluminescent 'searchlights'. Red coloration is seen at shallower depths, however, although often only on the opaque portions of transparent organisms (e.g. various pteropods, hydromedusae, salps, cephalopods, copepods) (Herring & Roe 1988). Whether this coloration is related to the crypticity predictions in this study depends on the visual thresholds in marine species.

Unfortunately, while the visual pigments of many marine teleosts and crustaceans have been characterized (Bowmaker 1990; Frank & Widder 1999; Marshall *et al.* 1999; Muntz 1999), the thresholds for vision and wavelength discrimination are poorly understood for marine species (Douglas & Hawryshyn 1990). The approximate irradiance threshold for human photopic (cone-based) vision is 10^{10} photons $cm^{-2}\ s^{-1}\ nm^{-1}$, with the threshold for scotopic (rod-based) vision at 10^7 photons $cm^{-2}\ s^{-1}\ nm^{-1}$ (Loew & McFarland 1990). The scotopic vision of mesopelagic fishes is *ca.* 10–100 times more sensitive than this (Douglas & Hawryshyn 1990), and examples exist of photopic vision considerably more sensitive than human vision. In goldfish, both rod and red-sensitive cones operate at the absolute vision threshold (Powers & Easter 1978). Certain mesopelagic fishes with multi-banked retinae may possess colour discrimination which uses a single

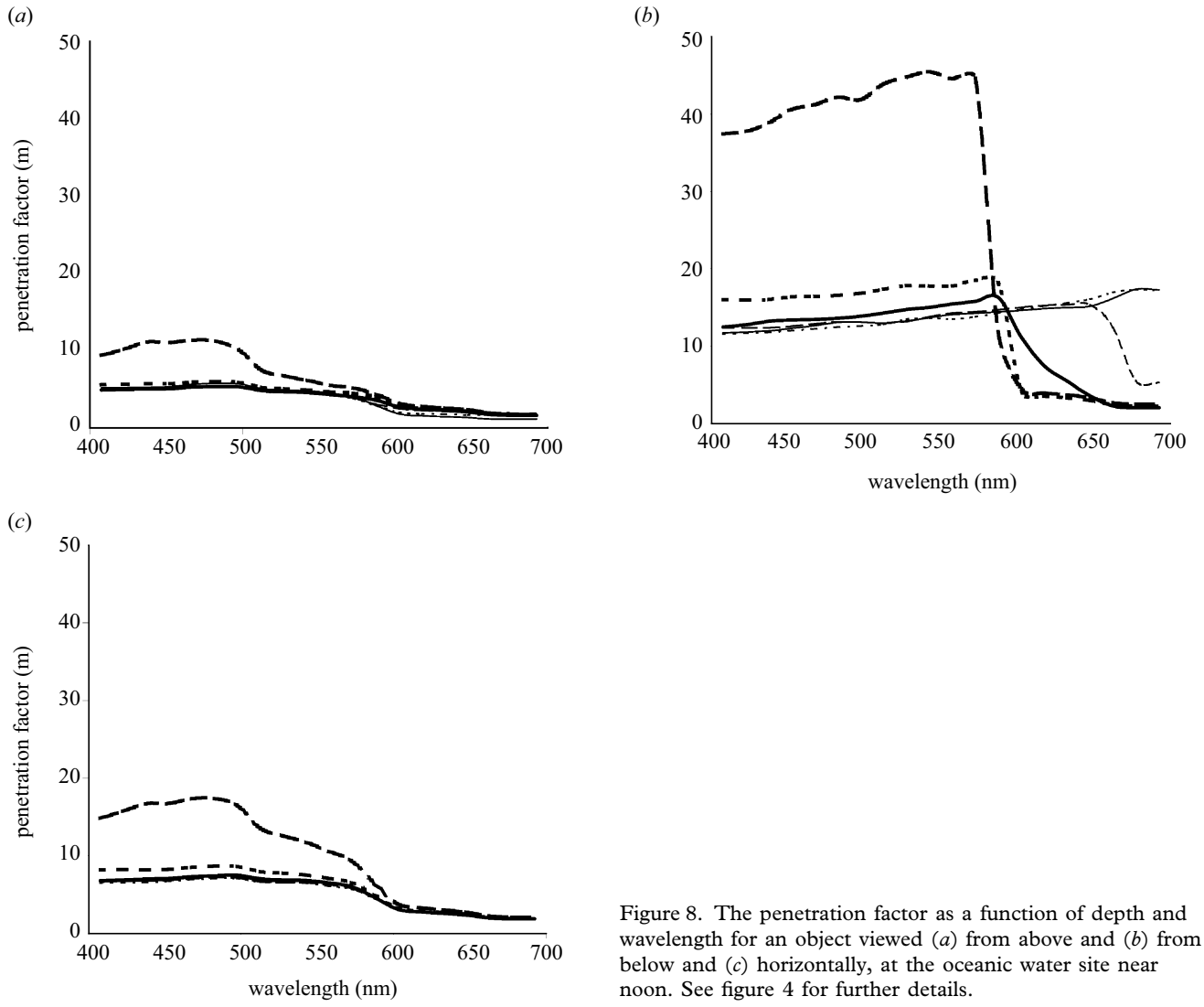

Figure 8. The penetration factor as a function of depth and wavelength for an object viewed (*a*) from above and (*b*) from below and (*c*) horizontally, at the oceanic water site at noon. See figure 4 for further details.

rod pigment, because the banks farther from the cornea receive light that has been filtered by passage through preceding banks (Denton & Locket 1989). Thickened retinas are also known to broaden the spectral response of the visual system (Partridge & Cummings 1999). There are also visual systems that contain two different types of rods, with different peak sensitivities, allowing colour vision at scotopic light intensities (Makino-Tasaka & Suzuki 1984). Given the selective pressures of visual predation, further examples of low-light level colour discrimination in the midwater realm are expected.

However, as mentioned above, colour discrimination is a sufficient, but unnecessary condition for detection of non-optimal crypticity in the red. In most cases, significant visual sensitivity in the red, even with one pigment, suffices. In this case, an organism that is cryptic at shorter wavelengths, but not cryptic at red wavelengths can be detected, not as red, but as an intensity mismatch. Given the paucity of visual pigments at extremely long wavelengths in marine species (Marshall *et al.* 1999; Muntz 1999; Partridge & Cummings 1999), it is unlikely that chlorophyll fluorescence, which peaks at 675 nm, has any visual relevance. The inelastically scattered light, however, causes significant effects at wavelengths as low as 550 nm, and may be relevant to species with well-developed low-light vision.

(c) *Effects of viewing angle*

A surprising result of this study is that reflectance of the ventral surface has little to no effect on an organism's visibility. Even in the limiting case of horizontal viewing of the ventral surface, the sighting distance for white coloration is 80% of the sighting distance for black coloration over most of the spectral range. It is only at the higher wavelengths, where little vision may occur, that a significant effect on sighting distance is observed, and then only for horizontal viewing. White ventral coloration is common in marine organisms (Cott 1940) and, while it has been known for some time that it could not be completely cryptic (reviewed by Kiltie 1988), the fact that it is not cryptic at all has not been mentioned, although it is well known that downward radiances are at least 200 times greater than upward radiances (Denton 1990). One possible explanation is that the minimum contrast thresholds of some marine visual predators and prey are considerably higher than 0.02. For example, if the minimum contrast threshold equals 0.2, then the sighting distance for a white ventral surface would be half that for a black ventral

surface for horizontal viewing, rather than 80%. However, the ratio for viewing from below would still be very close to unity (greater than 99%). A more likely explanation includes the fact that the surfaces of many marine organisms are curved. While a completely horizontal white surface offers little benefit (due to its low irradiance), one that is angled (so that its irradiance is higher) is more beneficial. As the angle increases from horizontal to vertical, the benefit of white coloration increases until the predicted reflectance drops below unity for some wavelengths. Above this critical angle (determined by the radiance distribution and the viewing angle), coloured surfaces will be more cryptic. This explanation, however, does not account for the white ventral surfaces of dorsoventrally flattened animals such as rays, suggesting the possibility that white ventral coloration serves no optical purpose in some marine species, as has been suggested by Kiltie (1988). The white coloration of animals in completely aphotic environments, such as caves, lends further support to this possibility.

(**d**) *Effects of viewing azimuth in horizontal lines of sight*

The differences between the predictions for the two different azimuths are due to the fact that the azimuth affects the background radiance and the irradiance at the organism's surface. Viewing in the solar azimuth increases the background radiance and decreases the organism's radiance, due to the lower irradiance at its surface. The opposite is true for viewing opposite the solar azimuth. The differences in predicted cryptic coloration were relatively minor, however, even in cases with low solar elevation. Of course, for specularly reflective surfaces (i.e. mirrored), the effects of azimuth would be considerably more pronounced (Denton 1970).

The predictions in conspicuous coloration at shallow depths, however, were strongly dependent on viewing azimuth, due to the sharp change in predicted reflectance from unity to zero when the predicted cryptic reflectance equalled one-half. Cephalopods and other species that can rapidly change body coloration may be able to take advantage of this azimuthal effect. Also, species searching for a conspicuous signal (e.g. species recognition patterns) would increase their chances of success by viewing in multiple azimuths.

(**e**) *Effects of solar elevation*

Except in the case of the upward viewing angle (where predicted reflectances for crypticity were well beyond the physically realizable value of unity), the effect of solar elevation was relatively minor. This is due to the fact that, while the overall radiant intensity is affected by solar elevation, the radiance distribution is only slightly changed. This is due to the refraction at the sea–air interface (which decreases the range of solar elevations to 0–47.5°), light scattering by water and particles, and strong absorption by water (which tends to increase intensity at the zenith and decrease it at larger angles, due to path length differences).

In this study, the lower solar elevation was above the horizon, therefore the strong changes in the spectrum of skylight during twilight reported by Munz & McFarland (1977) and others were not considered. However, with the exception of wavelength altering processes (e.g. Raman scattering, fluorescence), the sky irradiance has no effect on the predictions for crypticity or conspicuity, because it equally effects the entire spatial radiance distribution at a given wavelength. For example, if, as the sun sets, the sky becomes relatively richer in short wavelengths, both the downward radiance and the upwelling irradiance become richer in the same proportion and the *optimal* reflectance for crypticity in the downward viewing angle (which is a ratio of the two) remains unchanged. While this at first appears to be at odds with numerous studies describing the changing spectrum at twilight and its effects on visual predation (e.g. Munz & McFarland 1977; Endler 1991; McFarland *et al.* 1999), this is because these studies involve objects that are not optimally cryptic. Because any naturally cryptic animal will almost certainly have some contrast at certain wavelengths, the viewer will perceive colour and/or contrast changes as twilight approaches. In addition, crepuscular and nocturnal visual systems have different spectral sensitivities and minimum contrast thresholds compared to diurnal systems, which also alters the appearance and detectability of the object (Douglas & Hawryshyn 1990; Siriraksophon & Morinaga 1996). Therefore, while the skylight illumination has little to no effect on the *optimal* reflectance for crypticity, it can affect the visibility of non-optimally cryptic animals. This is analogous to the fact that, while a white card on a white background is undetectable under any form of illumination, a slightly pink card will be more detectable under red illumination than under blue.

(**f**) *Effects of depth and viewing angle on the attenuation of contrast*

As described above, the sighting distance of an organism depends on both its inherent contrast and on the attenuation properties of the water. The latter property, referred to here as the penetration factor, also strongly depends on wavelength, depth, and most importantly, viewing angle. In general, this factor is highest for the upward viewing angle, though it is not necessarily highest at the wavelength of greatest light transmission, because it depends on the difference between the beam attenuation and diffuse attenuation coefficient. For other viewing angles, it peaks at the wavelength of maximum transmission. It is relatively unaffected by solar elevation and completely unaffected by azimuth for horizontal viewing.

Because the contrast factor is a logarithmic function (and therefore increases slowly), and because the dependence of the penetration factor on viewing angle is large, it often occurs that the viewing angle with the least inherent contrast has the longest sighting distance. For example, in the oceanic water sample, the inherent contrast for a conspicuously coloured individual viewed from above was roughly two orders of magnitude higher than the inherent contrast viewed from below. However, the distance at which the apparent contrast had decreased to 0.01 was roughly twice as far for the latter than for the former.

A second interesting characteristic of the upward viewing angle is that the wavelength of least contrast attenuation is significantly displaced from the wavelength of least light attenuation (figure 8*b*). This is due to the fact that contrast attenuation in the upward viewing angle depends on the difference between the beam and downward

Table 1. Summary of the effects of various parameters on the predictions for crypticity, conspicuity, and penetration factor.

effects of	on crypticity predictions	on conspicuity predictions	on penetration factor
depth	substantial: dorsal coloration near the surface is a darkened hue of the water's colour, changing to red with increasing depth. Lateral coloration is approximately independent of azimuth and similar to dorsal coloration, though lighter. Ventral coloration is white, though white is often only slightly more cryptic than black.	substantial: dorsal coloration is white near surface, changing to light blue and then blue with increasing depth. Lateral coloration depends strongly on azimuth. Lateral coloration viewed in the solar azimuth is a complex function of depth. Lateral coloration viewed opposite the solar azimuth approximates dorsal coloration. Ventral coloration is black, though black is often only slightly more conspicuous than white.	moderate: all penetration factors depend only slightly on depth except at large depths in oceanic water or when viewed from below.
solar elevation	minor: insignificant effect on dorsal coloration. Lateral coloration is slightly more dependent on azimuth at low solar elevations than at high. White ventral coloration is no more cryptic at low solar elevations.	minor: minor effect on dorsal and lateral coloration. Black ventral coloration is no more conspicuous at high solar elevations.	minor: penetration factor is essentially independent of solar elevation, except for a slight decrease (10–20%) at low solar elevations when viewed from below.

radiance attenuation coefficients, which is not necessarily minimal at the wavelength of greatest light penetration. Also, the apparent contrast of conspicuously coloured objects is generally greatest at longer wavelengths for all viewing angles, particularly at short distances from the object, due to the fact that the inherent contrast is higher (figure 6). These results are in agreement with Lythgoe's contrast hypothesis (e.g. Lythgoe & Partridge 1989), which suggested that the reason many visual pigments are offset from the wavelength of peak light penetration was to maximize the perceived contrast of underwater objects.

However, the actual sighting distances shown in figure 6 are almost certainly overestimates, even for large objects. Several image degrading factors, such as large- and small-scale refractive index fluctuations (due to variations in temperature and salinity), and the presence of large particles (e.g. marine snow) are not measurable using currently available instruments. Although these factors have a significant effect on the magnitudes of the sighting distances, they probably have little effect on the dependencies on wavelength and viewing angle.

(g) *Primary conclusions and cautions*

The effects of viewing angle and depth on the predictions for crypticity and conspicuity were substantial, often non-intuitive, and interacted in a complex fashion (figure 5; table 1). The effects of viewing azimuth were less significant and the effects of solar elevation were generally minor. In general the ratio of downwelling to upwelling light intensity was far too high for white ventral coloration to provide any significant cryptic benefit. Although objects viewed from below had the lowest inherent contrasts, they also had the highest penetration factors (though not at the wavelengths of greatest light penetration), resulting in the highest sighting distances. Inherent contrast and apparent contrast at short distances for conspicuously coloured objects was highest at wavelengths displaced from the wavelength of maximum light penetration, consistent with Lythgoe's contrast hypothesis.

Although mentioned above, it bears repeating that, because this study does not include the sensitivity, colour discrimination, and minimum contrast thresholds of a given animal, it presents the location of optima, but not the gradient surrounding them. Given departures from a particular optimum will have varying effects on the animal's detectability depending on what is viewing it. For example, the increase in predicted long-wavelength reflectance with depth is irrelevant to an animal interacting only with species that cannot see in this region. The predictions in this study form a physical background that must be combined with particular visual parameters to make conclusions about specific cases.

The author thanks Dr John Endler, Dr Tamara Frank, Dr William Kier, Dr Marianne Moore and Dr Edith Widder for comments on the manuscript, and Dr Andrew Barnard, Dr W. Scott Pegau and Dr Ronald Zaneveld for generously providing data on inherent optical properties and chlorophyll concentrations. The author also thanks Dr Michael Neubert for discussions on the proof in Appendix A. This work was funded by a grant from the Rinehart Coastal Research Center to Dr Laurence P. Madin and S.J., and by a Woods Hole Oceanographic Institution Postdoctoral Scholarship to S.J.

APPENDIX A

The problem is to show under what circumstances the integral of a non-zero contrast function, $C(\lambda)$, weighted by two different non-zero visual response curves can equal zero. Let $V(\lambda)$ and $V'(\lambda)$ be two different visual response curves. Then,

$$C = \int_{\lambda_1}^{\lambda_N} C(\lambda)\, V(\lambda)\, \mathrm{d}\lambda = 0, \quad \text{and} \tag{A 1}$$

$$C' = \int_{\lambda_1}^{\lambda_N} C(\lambda) V'(\lambda) \mathrm{d}\lambda = 0. \quad \text{(A 2)}$$

Approximate the three continuous functions as N-dimensional vectors, $\boldsymbol{C}(\lambda_1, \lambda_2, \ldots \lambda_N)$, $\boldsymbol{V}(\lambda_1, \lambda_2, \ldots \lambda_N)$, and $\boldsymbol{V''}(\lambda_1, \lambda_2, \ldots \lambda_N)$. Then,

$$C = \int_{\lambda_1}^{\lambda_N} C(\lambda) V(\lambda) \mathrm{d}\lambda = \sum_{1}^{N} C_i V_i \Delta\lambda = \boldsymbol{C} \cdot \boldsymbol{V} \Delta\lambda = 0, \quad \text{and} \quad \text{(A 3)}$$

$$C' = \int_{\lambda_1}^{\lambda_N} C(\lambda) V'(\lambda) \mathrm{d}\lambda = \sum_{1}^{N} C_i V_i' \Delta\lambda = \boldsymbol{C} \cdot \boldsymbol{V'} \Delta\lambda = 0, \quad \text{(A 4)}$$

where $\cdot$ is the dot product of two vectors, which, when the vectors are non-zero, equals zero only when the vectors are perpendicular. Therefore $\boldsymbol{C}$ must be perpendicular to both $\boldsymbol{V}$ and $\boldsymbol{V'}$. This places stringent limitations on $\boldsymbol{C}$, which increase as additional visual response curves (e.g. $\boldsymbol{V''}$, $\boldsymbol{V'''}$) are considered. In addition, because all visual response curves are positive, $\boldsymbol{C}$ will be neither all positive nor all negative (because it is a perpendicular), but will cross zero an average of $(N - 1)/2$ times, and therefore have an average of $((N - 1)/2) - 1$ peaks. Natural pigments and light sources rarely have more than two peaks. Therefore, while a non-zero contrast function that results in zero contrast when integrated over different visual systems is theoretically possible, it is likely to be physically unrealizable.

REFERENCES

Aksnes, D. L. & Giske, J. 1993 A theoretical model of aquatic visual feeding. *Ecol. Model* **67**, 233–250.

Bakker, T. C. M. & Mundwiler, B. 1992 Female mate choice and male red coloration in a natural three-spined stickleback (*Gasterosteus aculeatus*) population. *Behav. Ecol.* **5**, 74–80.

Bowmaker, J. K. 1990 Visual pigments of fishes. In *The visual system of fish* (ed. R. H. Douglas & M. B. A. Djamgoz), pp. 81–107. New York: Chapman & Hall.

Bowmaker, J. K. & Kunz, Y. W. 1987 Ultraviolet receptors, tetrachromatic colour vision, and retinal mosaics in the brown trout (*Salmo trutta*): age-dependent changes. *Vis. Res* **27**, 2102–2108.

Browman, H. I., Novales-Flamarique, I. & Hawryshyn, C. W. 1994 Ultraviolet photoreception contributes to prey search behaviour in two species of zooplanktivorous fishes. *J. Exp. Biol.* **186**, 187–198.

Chapman, G. 1976 Reflections on transparency. In *Coelenterate ecology and behavior* (ed. G. O. Mackie), pp. 491–498. New York: Plenum.

Cott, H. B. 1940 *Adaptive coloration in animals*. London: Methuen.

Crook, A. C. 1997 Colour patterns in a coral reef fish. Is background complexity important? *J. Exp. Mar. Biol. Ecol.* **217**, 237–252.

Denton, E. J. 1970 On the organization of reflecting structures in some marine animals. *Phil. Trans. R. Soc.* B **258**, 285–313.

Denton, E. J. 1990 Light and vision at depths greater than 200 metres. In *The visual system of fish* (ed. R. H. Douglas & M. B. A. Djamqoz), pp. 127–148. New York: Chapman & Hall.

Denton, E. J. & Locket, N. A. 1989 Possible wavelength discrimination by multibank retinae in deep-sea fishes. *J. Mar. Biol. Assoc. UK* **69**, 409–435.

Denton, E. J., Gilpin-Brown, J. B. & Wright, P. G. 1972 The angular distribution of the light produced by some mesopelagic fish in relation to their camouflage. *Proc. R. Soc. Lond.* B **182**, 145–158.

Douglas, R. H. & Hawryshyn, C. W. 1990 Behavioral studies of fish vision: an analysis of visual capabilities. In *The visual system of fish* (ed. R. H. Douglas & M. B. A. Djamgoz), pp. 373–418. New York: Chapman & Hall.

Endler, J. A. 1978 A predators view of animal colour patterns. *Evol. Biol.* **11**, 319–364.

Endler, J. A. 1983 Natural and sexual selection on colour patterns in poeciliid fishes. *Environ. Biol. Fish* **9**, 173–190.

Endler, J. A. 1990 On the measurement and classification of colour in studies of animal colour patterns. *Biol. J. Linn. Soc.* **41**, 315–352.

Endler, J. A. 1991 Variations in the appearance of guppy colour patterns to guppies and their predators under different visual conditions. *Vis. Res.* **31**, 587–608.

Ferguson, G. P. & Messenger, J. B. 1991 A countershading reflex in cephalopods. *Proc. R. Soc. Lond.* B **243**, 63–67.

Frank, T. M. & Widder, E. A. 1999 Comparative study of the spectral sensitivities of mesopelagic crustaceans. *J. Comp. Physiol.* A **185**, 255–265.

Fuiman, L. A. & Magurran, A. E. 1994 Development of predator defenses in fishes. *Rev. Fish. Biol. Fish* **4**, 145–183.

Giske, J., Aksnes, D. L. & Fiksen, O. 1994 Visual predators, environmental variables and zooplankton mortality risk. *Vie Milieu* **44**, 1–9.

Gordon, H. R. 1999 Contributions of raman scattering to water-leaving radiance: a reexamination. *Appl. Opt.* **38**, 3166–3174.

Gregg, W. W. & Carder, K. L. 1990 A simple spectral solar irradiance model for cloudless maritime atmospheres. *Limnol. Oceanogr.* **35**, 1657–1675.

Hanlon, R. T. & Messenger, J. B. 1996 *Cephalopod behavior*. Cambridge University Press.

Hamner, W. M. 1996 Predation, cover, and convergent evolution in epipelagic oceans. In *Zooplankton: sensory ecology and physiology* (ed. P. H. Lenz, D. K. Hartline, J. E. Purcell & D. L. Macmillan), pp. 17–37. Amsterdam: Overseas Publishers Association.

Harrison, A. W. & Coombes, C. A. 1988 An opaque cloud cover model of sky short wavelength radiance. *Sol. Energy* **41**, 387–392.

Hemmings, C. C. 1975 The visibility of objects underwater. In *Light as an ecological factor* (ed. G. C. Evans, T. Bainbridge & O. Rackhman), pp. 359–374. Oxford: Blackwell.

Herring, P. J. 1967 The pigments of plankton at the sea surface. *Symp. Zool. Soc. Lond.* **19**, 215–235.

Herring, P. J. 1973 Depth distribution of the carotenoid pigments and lipids of some oceanic animals. 2. Decapod crustaceans. *J. Mar. Biol. Assoc. UK* **53**, 539–562.

Herring, P. J. & Roe, H. S. J. 1988 The photoecology of pelagic oceanic decapods. *Symp. Zool. Soc. Lond.* **59**, 263–290.

Hester, F. J. 1968 Visual contrast thresholds of the goldfish *Carassius auratus*. *Vis. Res.* **8**, 1315–1335.

Jerlov, N. G. 1976 *Marine optics*. New York: Elsevier.

Johnsen, S. & Widder, E. A. 1998 The transparency and visibility of gelatinous zooplankton from the northwestern Atlantic and Gulf of Mexico. *Biol. Bull.* **195**, 337–348.

Johnsen, S. & Widder, E. A. 1999 The physical basis of transparency in biological tissue: ultrastructure and the minimization of light scattering. *J. Theor. Biol.* **199**, 181–198.

Johnsen, S. & Widder, E. A. 2001 Ultraviolet absorption in transparent zooplankton and its implications for depth distribution and visual predation. *Mar. Biol.* **138**, 717–730.

Kiltie, R. A. 1988 Countershading: universally deceptive or deceptively universal? *Trends Ecol. Evol.* **3**, 21–23.

Kirk, J. T. O. 1983 *Light and photosynthesis in aquatic ecosystems*. Cambridge University Press.

Loew, E. R. & Lythgoe, J. N. 1978 The ecology of cone pigments in teleost fishes. *Vis. Res.* **18**, 715–722.

Loew, E. R. & McFarland, W. N. 1990 The underwater visual environment. In *The visual system of fish* (ed. R. H. Douglas & M. B. A. Djamgoz), pp. 1–44. New York: Chapman & Hall.

Loew, E. R., McFarland, W. N., Mills, E. L. & Hunter, D. 1993 A chromatic action spectrum for planktonic predation by juvenile yellow perch, *Perca flavescens*. *Can. J. Zool.* **71**, 384–386.

Lythgoe, J. N. 1979 *The ecology of vision*. Oxford: Clarendon.

Lythgoe, J. N. 1984 Visual pigments and environmental light. *Vis. Res.* **24**, 1539–1550.

Lythgoe, J. N. & Partridge, J. C. 1989 Visual pigments and the acquisition of visual information. *J. Exp. Biol.* **146**, 1–20.

McAllister, D. E. 1967 The significance of ventral bioluminescence in fishes. *J. Fish. Res. Bd Can.* **24**, 537–554.

McFall-Ngai, M. J. 1990 Crypsis in the pelagic environment. *Am. Zool.* **30**, 175–188.

McFarland, W. N., Wahl, C., Suchanek, T. & McAlary, F. 1999 The behavior of animals around twilight with emphasis on coral reef communities. In *Adaptive mechanisms in the ecology of vision* (ed. S. N. Archer, M. B. A. Djamgoz, E. R. Loew, J. C. Partridge & S. Vallerga), pp. 583–628. Boston: Kluwer.

Maffione, R. A., Voss, J. M. & Mobley, C. D. 1998 Theory and measurements of the complete beam spread function of sea ice. *Limnol. Oceanogr.* **43**, 34–43.

Makino-Tasaka, M. & Suzuki, T. 1984 The green rod pigment of the bullfrog, *Rana catesbeiana*. *Vis. Res.* **24**, 309–322.

Marshall, N. J. 2000 Communication and camouflage with the same 'bright' colours in reef fishes. *Phil. Trans. R. Soc. Lond.* B **355**, 1243–1248.

Marshall, B. R. & Smith, R. C. 1990 Raman scattering and in-water optical properties. *Appl. Opt.* **29**, 71–84.

Marshall, N. J., Kent, J. & Cronin, T. W. 1999 Visual adaptations in crustaceans: spectral sensitivity in diverse habitats. In *Adaptive mechanisms in the ecology of vision* (ed. S. N. Archer, M. B. A. Djamgoz, E. R. Loew, J. C. Partridge & S. Vallerga), pp. 285–328. Boston: Kluwer.

Mertens, L. E. 1970 *In-water photography: theory and practice*. New York: Wiley.

Mobley, C. D. 1995 The optical properties of water. In *Handbook of optics*, vol. 1 (ed. M. Bass, E. W. Van Strylan, D. R. Williams & W. L. Wolfe), pp. 43.1–43.56. New York: McGraw-Hill Inc.

Mobley, C. D., Gentili, B., Gordon, H. R., Jin, Z., Kattawar, G. W., Morel, A., Reinersman, P., Stamnes, K. & Stavn, R. H. 1993 Comparison of numerical models for computing underwater light fields. *Appl. Opt.* **32**, 7484–7504.

Muntz, W. R. A. 1990 Stimulus, environment and vision in fishes. In *The visual system of fish* (ed. R. H. Douglas & M. B. A. Djamgoz), pp. 491–511. New York: Chapman & Hall.

Muntz, W. R. A. 1999 Visual systems, behavior and environment in cephalopods. In *Adaptive mechanisms in the ecology of vision* (ed. S. N. Archer, M. B. A. Djamgoz, E. R. Loew, J. C. Partridge & S. Vallerga), pp. 467–484. Boston: Kluwer.

Munz, F. W. & McFarland, W. N. 1973 The significance of spectral position in the rhodopsin of tropical marine fishes. *Vis. Res.* **13**, 1829–1874.

Munz, F. W. & McFarland, W. N. 1977 Evolutionary adaptations of fishes to the photic environment. In *The visual system of vertebrates* (ed. F. Crescitelli), pp. 194–274. New York: Springer.

Palmer, J. M. 1995 The measurement of transmission, absorption, emission, and reflection. In *Handbook of optics*, vol. 2 (ed. M. Bass, E. W. van Strylan, D. R. Williams & W. L. Wolfe), pp. 25.1–25.25. New York: McGraw-Hill.

Partridge, J. C. & Cummings, M. E. 1999. In *Adaptive mechanisms in the ecology of vision* (ed. S. N. Archer, M. B. A. Djamgoz, E. R. Loew, J. C. Partridge & S. Vallerga), pp. 251–284. Boston: Kluwer.

Petzold, T. J. 1977 Volume scattering functions for selected ocean waters. In *Light in the sea* (ed. J. E. Tyler), pp. 150–174. Stroudsberg: Dowden, Hutchinson and Ross.

Pope, R. M. & Fry, E. S. 1997 Absorption spectrum (380–700 nm) of pure water. II. Integrating cavity measurements. *Appl. Opt.* **36**, 8710–8723.

Powers, M. K. & Easter, S. S. 1978 The absolute visual sensitivity of the goldfish. *Vis. Res.* **18**, 1137–1147.

Prieur, L. & Sathyendranath, S. 1981 An optical classification of coastal and oceanic waters based on the specific spectral absorption curves of phytoplankton pigments, dissolved organic matter, and other particulate materials. *Limnol. Oceanogr.* **26**, 671–689.

Purcell, J. E. 1980 Influence of siphonophore behavior on their natural diets; evidence for aggressive mimicry. *Science* **209**, 1045–1047.

Seapy, R. R. & Young, R. E. 1986 Concealment in epipelagic pterotracheid heteropods (Gastropoda) and cranchiid squids (Cephalopoda). *J. Zool.* **210**, 137–147.

Shashar, N., Hanlon, R. T. & Petz, A. 1998 Polarization vision helps detect transparent prey. *Nature* **393**, 222–223.

Siriraksophon, S. & Morinaga, T. 1996 Effect of background brightness on the visual contrast threshold of the Japanese common squid. *Fish Sci.* **62**, 534–537.

Siriraksophon, S., Nakamura, Y. & Matsuike, K. 1995 Visual contrast threshold of Japanese common squid *Todarodes pacificus* Steenstrup. *Fish Sci.* **61**, 574–577.

Stavn, R. H. & Wiedemann, A. D. 1988 Optical modeling of clear ocean light fields: Raman scattering effects. *Appl. Opt.* **27**, 4002–4011.

Stramska, M., Stramski, D., Mitchell, B. G. & Mobley, C. D. 2000 Estimation of the absorption and backscattering coefficients from in-water radiometric measurements. *Limnol. Oceanogr.* **45**, 628–641.

Waterman, T. H. 1981 Polarization sensitivity. In *Handbook of sensory physiology*, vol. 7/6B (ed. H. Autrum), pp. 281–469. New York: Springer.

Widder, E. A., Latz, M. I. & Case, J. F. 1983 Marine bioluminescence spectra measured with an optical multichannel detection system. *Biol. Bull.* **165**, 791–810.

Wyszecki, G. & Stiles, W. S. 1982 *Colour science: concepts and methods, quantitative data and formulae*. New York: Wiley.

As this paper exceeds the maximum length normally permitted, the author has agreed to contribute to production costs.